Water Behavior in Mesoporous Materials As Studied by NMR Relaxometry

ARTICLE *in* THE JOURNAL OF PHYSICAL CHEMISTRY A · AUGUST 2011

Impact Factor: 2.69 · DOI: 10.1021/jp205456g · Source: PubMed

4 AUTHORS, INCLUDING:

Emilie Steiner
Karolinska Institutet
7 PUBLICATIONS **46** CITATIONS
SEE PROFILE

Sabine Bouguet-Bonnet
University of Lorraine
24 PUBLICATIONS **395** CITATIONS
SEE PROFILE

Daniel Canet
University of Lorraine
302 PUBLICATIONS **3,858** CITATIONS
SEE PROFILE

THE JOURNAL OF PHYSICAL CHEMISTRY A

ARTICLE

pubs.acs.org/JPCA

Water Behavior in Mesoporous Materials As Studied by NMR Relaxometry

Emilie Steiner,[†] Sabine Bouguet-Bonnet,[†] Jean-Luc Blin,[‡] and Daniel Canet*[,†]

[†]Méthodologie RMN (CRM2, UMR 7036 CNRS) and [‡]Physicochimie des Colloïdes (SRSMC, UMR 7565 CNRS), Faculté des Sciences et Technologies, Nancy-Université, BP 70239, 54506 Vandœuvre-lès-Nancy Cedex, France

Supporting Information

ABSTRACT: Water in mesoporous materials possessing a two-dimensional hexagonal structure has been studied by the variation of its NMR longitudinal relaxation time T_1 as a function of the static magnetic field value, or equivalently of the NMR measurement frequency. This technique, dubbed relaxometry, has been applied from 5 kHz (measurement frequency) up to 400 MHz with various instruments including a variable-field spectrometer operating between 8 and 90 MHz. Moreover, the range 0−5 kHz could be investigated by transverse relaxation, T_2 denoting the corresponding relaxation time, and relaxation in the rotating frame, $T_{1\rho}$ denoting the corresponding relaxation time. Measurements of proton relaxation rates (inverse of relaxation times) have been performed with H_2O and HOD (residual protons of heavy water) at water volumes of 80%, 60%, and 40% relative to the porous volume. Comparison between H_2O and HOD shows clearly that, above 1 MHz where both sets of data are superposed, relaxation is purely intermolecular and due to paramagnetic relaxation (dipolar interactions of water protons with unpaired electrons of paramagnetic entities). Below 1 MHz, it is possible to subtract the intermolecular contribution (given by HOD data) from H_2O data so that one is left with intramolecular relaxation which is solely due to water reorientational motions. The analysis of these low-frequency data (in terms of Lorentzian functions) reveals two types of water within the pores: one interacting strongly with the surface and the other corresponding to a second layer. High-frequency data, which arise from paramagnetic relaxation, exhibit again two types of water. Due to their correlation times, one type is assigned to relatively free water within the pores while the other type corresponds to bulk (interparticular) water. Their proportions, given as a function of the volume fraction, are consistent with the above assignments.

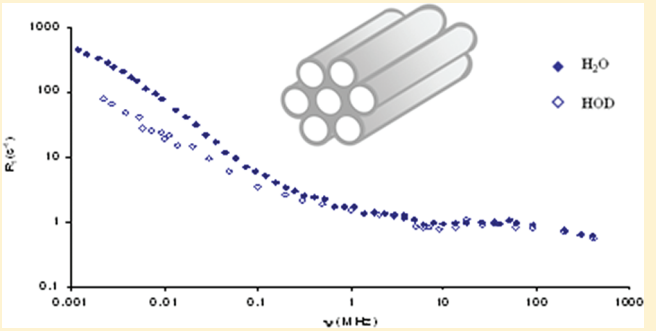

INTRODUCTION

It is well-known that nuclear spin relaxation times, as measured by NMR, provide valuable information about molecular motions.[1,2] However, whenever these motions are fast enough, the so-called extreme narrowing conditions prevail. In that case, relaxation times (or their inverse, called relaxation rates) do not depend on the measurement frequency, that is, on the value of the NMR static magnetic field, and this entails the loss of some dynamical information. Conversely, in the case of sufficiently slow molecular dynamics, relaxation rates become frequency-dependent, and the analysis of their evolution yields interesting pieces of information that could not be obtained by other techniques. This occurs provided that the quantity $4\pi^2\nu^2\tau_c^2$ is comparable to or greater than unity (ν is the measurement frequency and τ_c is an effective correlation time describing the relevant motion). The technique, which consists of measuring the longitudinal rate R_1 (the inverse of the relaxation time T_1) as a function of the measurement frequency, is called relaxometry.[3,4] Results are generally presented in the form of dispersion curves (R_1 versus ν) and involve the broadest available frequency range. Relaxometry has been widely used for studying porous media.[5−7] The present work concerns particular porous media, called mesoporous materials, that possess a two-dimensional hexagonal array.[8] In fact, our system has been synthesized by protocols[9] that differ somewhat from those described in ref 8. These mesoporous materials are thought of as being constituted by infinitely long cylinders packed in a hexagonal arrangement. These materials are obtained in the form of porous powders that can be embedded with water. It is believed that part of the water penetrates into cylinders without any exchange with interparticular (intergranular) water. Our objective is to characterize the different types of water in these well-organized materials. To the best of our knowledge, these materials have not been investigated previously by relaxometry.

Our approach will rest exclusively on ^{1}H relaxometry, even if the matrix is embedded with D_2O. Several authors have used D_2O and ^{2}H relaxometry for the investigation of porous media.[10−13] However, ^{2}H relaxometry involves necessarily a limited frequency range because the gyromagnetic constant of deuterium is 13 times smaller than the proton gyromagnetic constant. On the other hand,

Received: June 10, 2011
Revised: July 26, 2011
Published: July 27, 2011

all relaxometers are not amenable to deuterium measurements (including ours; see Experimental Section). For these two reasons, we disregarded ^{2}H relaxometry and we rather looked at proton relaxometry of HOD (residual water molecules possessing one proton). It turns out that, in this case, proton relaxation is purely intermolecular (the H−D dipolar interaction is truly negligible). Thus, it is expected that comparison of the two dispersion curves (H_2O and HOD) will be rewarding. It must be noticed that this latter approach has been seldom employed.[14] Moreover, thanks to unique instrumentation and having recourse to transverse relaxation and relaxation in the rotating frame for very low frequencies, we were able to obtain full dispersion curves between 0 and 400 MHz.

EXPERIMENTAL SECTION

Synthesis and Characterization of Mesoporous Materials. Two-dimensional (2D) hexagonal mesoporous materials were obtained via a cooperative templating mechanism (CTM). First, a micellar solution of the nonionic fluorinated surfactant $C_8F_{17}C_2H_4(OC_2H_4)_9OH$ [labeled as $R_8^F(EO)_9$ and provided by Dupont] was prepared at 10 wt % in water. The pH of the solution was then adjusted to 2 by use of sulfuric acid. The tetramethoxysilane (TMOS) silica source was added drop by drop until the surfactant/silica molar ratio equals 0.5. After 1 h of stirring, the gel obtained was placed in a Teflon autoclave and was hydrothermally treated during 1 day at 100 °C. Nonionic surfactant was completely removed from the final product by ethanol extraction performed with a Soxhlet device (see Supporting Information).

The hexagonal channel array of mesoporous materials was confirmed by X-ray measurements, and the textural properties were determined by nitrogen adsorption−desorption measurements on samples degassed beforehand. The pore size was found to be 4.5 nm, the pore volume was 1.3 $cm^3 \cdot g^{-1}$, and the Brunauer−Emmett−Teller (BET) surface area was 940 $m^2 \cdot g^{-1}$.

Sample Peparation and NMR Measurements. Mesoporous materials were first degassed for 1 day in an air oven at 120 °C in order to remove residual water molecules. Porous matrix was introduced in small airtight capsules, and samples were prepared by adding pure or heavy water at different filling degrees (80%, 60%, and 40%, corresponding to the percentage of the pore volume). Finally, samples were placed for 1 day at 25 °C in a thermostated bath, allowing the fluid phase to equilibrate and, therefore, ensuring sample stability as long as required. These samples were subsequently inserted in 10 mm o.d. NMR tubes.

^{1}H NMR experiments were performed at 25 °C on mesoporous materials embedded with pure or heavy water. Relaxation rates R_1, $R_{1\rho}$, and R_2 were measured for both H_2O protons and residual protons in 99.99% D_2O. Longitudinal relaxation rates R_1 in the 5 kHz−10 MHz ^{1}H frequency range were obtained with a SMARtracer relaxometer (Stelar Company, Mede, Italy). The 10−90 MHz range was investigated by means of a homemade spectrometer equipped with a variable-field electromagnet according to experimental procedures previously described.[15] Moreover, conventional spectrometers, including a homemade spectrometer operating at 200 MHz and two Bruker Avance spectrometers operating at 300 and 400 MHz, were used for the high-field data.

Experiments performed with the relaxometer were carried out according to a fast field-cycling procedure. With the high-field instruments, proton relaxation rates R_1 were measured by inversion− or saturation−recovery sequences.

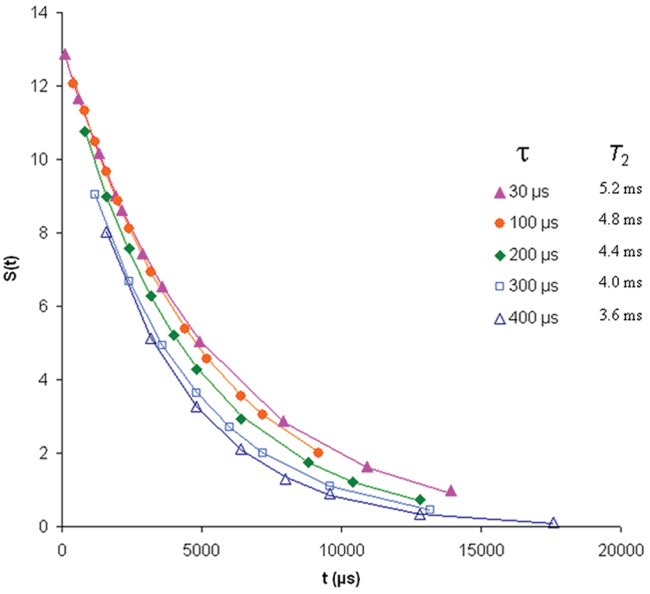

Figure 1. A series of CPMG decays of water in the 80% sample obtained for different values of τ listed in the inset (the number of 180° pulses is adjusted for probing the whole decay; experiments were performed with the homemade 200 MHz spectrometer). (Inset) Corresponding apparent T_2 values, which are seen to decrease regularly. The true T_2 is obtained by extrapolating these apparent values to $\tau = 0$.

Proton relaxation rates in the rotating frame $R_{1\rho}$ were measured with the 200 MHz homemade spectrometer by varying the duration of the spin locking field application. For obtaining the very low frequency dispersion curve, the spin locking field amplitude was varied from one experiment to the other and calibrated from the duration of the relevant 180° radio frequency (rf) pulse. Raw data were transformed by applying a procedure described in a previous paper[16] so that they can connect the conventional ^{1}H NMR dispersion curves down to the kilohertz frequency range. Transverse relaxation rate T_2 was measured according to the CPMG method[17] for compensating imperfections of the 180° rf pulses but also with different numbers of pulses in order to evaluate the importance of translational diffusion effects. These measurements are reported in Figure 1 in the form of decays corresponding to the parameters characterizing each CPMG sequence. Of course, when the number of 180° pulses is increased, the time interval τ between two consecutive pulses decreases. This should reveal a limit beyond which diffusion does not influence the apparent transverse relaxation time.[18] Indeed, Figure 1 shows such a result, which leads to (i) the true T_2 whenever the decay is no longer influenced by the number of pulses in the CPMG experiment, (ii) an estimation of the internal gradients that are responsible for the effect of translational diffusion on experimental data. This latter effect can be represented by an additional decay of the form $\exp(-2\gamma^2 g^2 D n \tau^3/3)$ where γ is the proton gyromagnetic constant, g is the internal gradient, D is the translational diffusion coefficient, and n is the number of pulses in the CPMG train. Finally, it can be stated that the evolution of the apparent T_2 cannot be ascribed to temperature effects arising from probe heating. If this was the case, monoexponential decays could not be observed, because this would occur when the number of pulses in the CPMG train increases.

In order to enhance the effect of diffusion in the presence of internal gradients, we performed additional CPMG experiments (Figure 2) with only one 180° pulse and by varying the interval

dx.doi.org/10.1021/jp205456g |J. Phys. Chem. A 2011, 115, 9941–9946

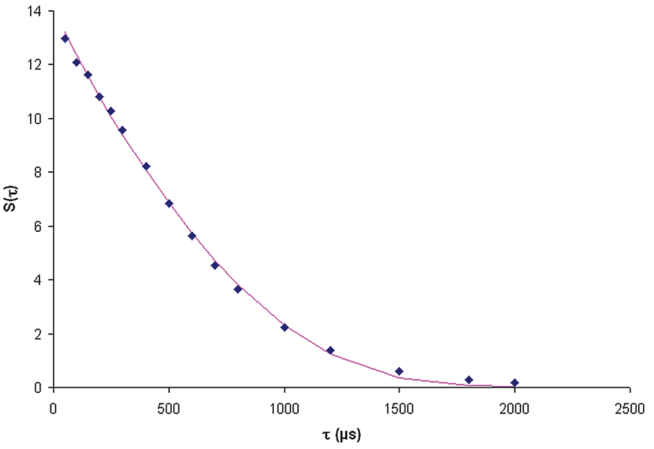

Figure 2. Experimental data (80% sample) of a Hahn experiment exhibiting a nonmonoexponential decay and thus the combined effects of diffusion in internal gradients and of transverse relaxation. Data could be fitted according to eq 1 (continuous curve).

τ (it is simply a Hahn echo). Thus, the decay obtained in such experimental conditions can be interpreted according to the following expression:

$$S(\tau) \propto \exp\left(-\frac{2\tau}{T_2}\right) \exp\left(-\frac{2}{3}\gamma^2 g^2 D\tau^3\right) \quad (1)$$

The internal gradient, g, was deduced from eq 1, assuming that D is the diffusion coefficient of pure water. Surprisingly enough, we found a large value (around 200 g·cm^{-1}), which of course precludes any diffusion measurement by conventional NMR equipment.

RESULTS

We were able to obtain full dispersion curves for all samples containing H_2O. The value at $\nu = 0$ is simply R_2 (inverse of T_2), whereas the values between 1 and 10 kHz were deduced from $R_{1\rho}$ (inverse of $T_{1\rho}$) by correcting these values according to the procedures described previously[16] in order to connect the R_1 dispersion curve. The H_2O experimental dispersion curves for the three filling degrees (80%, 60%, and 40%) are displayed in Figure 3.

In the case of the 80% sample, we were also able to obtain the full dispersion curve for HOD (Figure 4). Concerning the 60% and 40% samples, this turns out to be impossible for sensitivity reasons. Nevertheless, it can be noticed that, in all cases, H_2O and HOD dispersion curves perfectly coincide above 1 MHz. This unambiguously indicates that ^1H relaxation of H_2O is purely intermolecular, and this will be the key feature for our forthcoming analysis.

INTERPRETATION OF DISPERSION CURVES

Above 1 MHz. We first consider the high-frequency part of the dispersion curves (above 1 MHz), assuming that, in this frequency range, very low frequency components have nearly decayed to zero. From the considerations of the previous section, we can state that intermolecular dipolar interactions are overwhelming the intramolecular H−H dipolar interaction. Conversely, it is well-known that, in normal liquid water, the intermolecular contribution is about 25% of ^1H relaxation.[19]

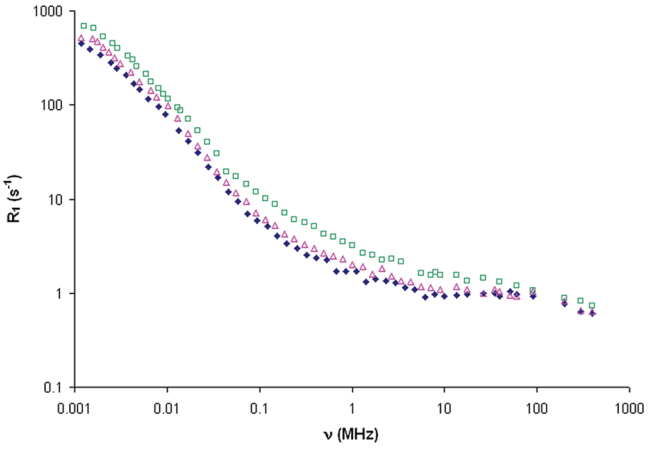

Figure 3. Full H_2O dispersion curves (1 kHz−400 MHz) for the three samples investigated here [(◆) 80%, (△) 60%, and (□) 40% filling degrees]. As the horizontal scale is logarithmic, it is impossible to represent R_2, which corresponds to the zero frequency.

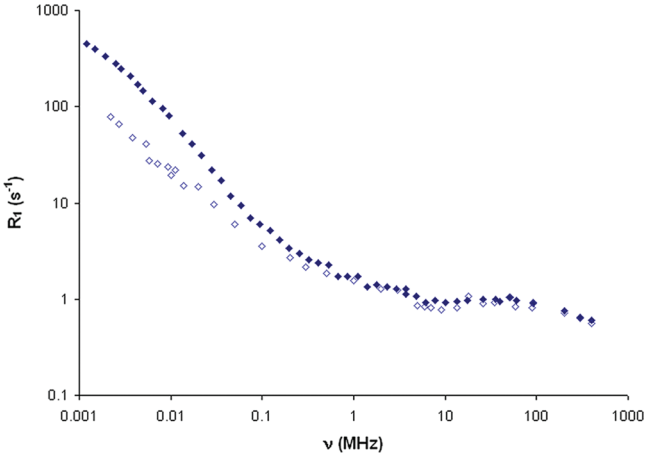

Figure 4. Comparison of (◆) H_2O and (◇) HOD dispersion curves for the 80% sample.

Since our experimental data are exclusively intermolecular and since the corresponding dipolar interactions cannot concern other water protons (one observes the same behavior with H_2O and D_2O), the only possible mechanism stems from dipolar interactions with unpaired electrons of paramagnetic species. Indeed, the experimental dispersion curves are characteristic of paramagnetic relaxation as observed in previous works.[15,20] It can be recalled that the high value of the electron gyromagnetic constant explains the frequency dependence of proton relaxation because the paramagnetic contribution to the longitudinal relaxation rate can be written (ω_e and ω_H being the electron and the proton resonance frequencies expressed in rad·s^{-1}) as

$$R_1^{\text{para}} = K^{\text{para}}[7\tilde{J}(\omega_e) + 3\tilde{J}(\omega_H)] \quad (2)$$

where K^{para} includes various constants, the amount of the considered species, and $1/r_{eH}^6$ (where r_{eH} is the distance between the unpaired electron and the considered proton). $\tilde{J}(\omega)$ is a normalized spectral density, its simplest form being

$$\tilde{J}(\omega) = \frac{2\tau_c}{1 + \omega^2\tau_c^2} \quad (3)$$

dx.doi.org/10.1021/jp205456g |J. Phys. Chem. A 2011, 115, 9941–9946

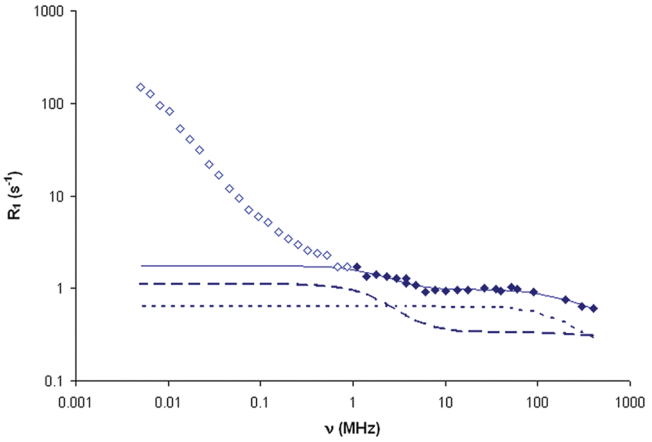

Figure 5. Decomposition of the experimental dispersion curve above 1 MHz (◆; 80% sample) into two Lorentzian functions (dashed and dotted plots). The continuous curve represents their superposition and is seen to fit perfectly the experimental data points.

Table 1. Parameters of the Two Lorentzian Functions That Fit the High-Frequency Part of the Dispersion Curve[a]

	filling degree		
	80%	60%	40%
$\tau_{c_1}^{para}$ (ns)	0.118	0.099	0.132
A_1^{para} (s^{-1})	0.111	0.155	0.270
$\tau_{c_2}^{para}$ (ns)	0.001	0.002	0.005
A_2^{para} (s^{-1})	0.063	0.058	0.068

[a] Above 1 MHz.

where τ_c is an effective correlation time including, among other things, the correlation time associated with the motion of the r_{eH} vector.

The description of the numerical procedures for analyzing dispersion curves will be deferred to a forthcoming publication. These procedures imply a decomposition in a series of Lorentzian curves,[21] each of them characterized by its amplitude and its correlation time (see eqs 2 and 3). For this high-frequency part of the dispersion curve, we find systematically two Lorentzian curves (Figure 5), fitted according to

$$R_1^{para} = A_1^{para}\left[\frac{7}{1+(\omega_e\tau_{c_1}^{para})^2}+\frac{3}{1+(\omega_H\tau_{c_1}^{para})^2}\right] + A_2^{para}\left[\frac{7}{1+(\omega_e\tau_{c_2}^{para})^2}+\frac{3}{1+(\omega_H\tau_{c_2}^{para})^2}\right] \quad (4)$$

Notice that the amplitudes A_i^{para} involve, among other things, the factor $2\tau_{c_i}^{para}$. The A_i^{para} and $\tau_{c_i}^{para}$ values are gathered in Table 1. Owing to the values of the correlation times, it is obvious that $\tilde{J}_i(\omega_H)$ lies in the extreme narrowing regime, while the frequency dependence arises from $\tilde{J}_i(\omega_e)$.

Nevertheless, one of the two correlation times ($\tau_{c_2}^{para}$) is in the picosecond range and therefore refers to free water. This type of water can be easily identified as interparticular (intergranular) water. Conversely, correlation times of 0.1 ns certainly characterize restricted motions for the corresponding water molecules.

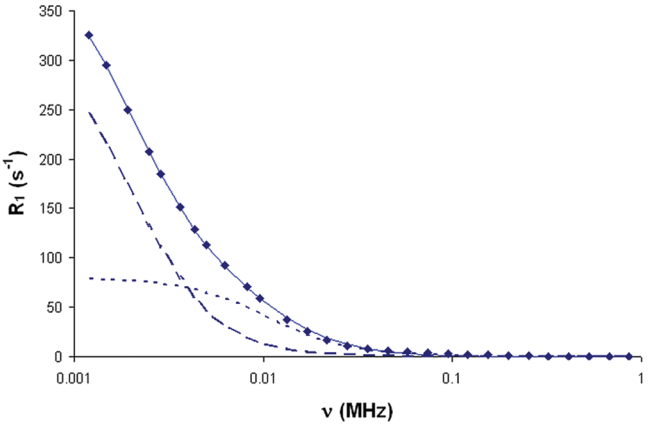

Figure 6. Low-frequency intramolecular part of the dispersion curve for the 80% sample (obtained by subtraction of the HOD curve from the H_2O curve; ◆). It can be decomposed into two Lorentzian functions (dashed and dotted plots). The continuous curve represents their superposition.

Table 2. Parameters of the Two Lorentzian Functions That Fit the Low-Field Frequency Part of the Dispersion Curve[a]

$\tau_{c_1}^{dip}$ (ns)	44 932
A_1^{dip} (s^{-1})	65.8
$\tau_{c_2}^{dip}$ (ns)	8408
A_1^{dip} (s^{-1})	15.8

[a] Obtained by subtraction of the HOD curve from the H_2O curve (80% sample).

Below 1 MHz. We shall concentrate on the 80% sample, for which H_2O and HOD full dispersion curves are available. Interpreting intermolecular contributions in the low-frequency range is not easy[22] and would anyway require a model.[23] We chose to subtract the HOD dispersion curve from the H_2O dispersion curve so as to be left with the H−H dipolar intramolecular contributions (Figure 6).

These contributions can be interpreted according to the following equation:

$$R_1^{dip} = K^{dip}5\tilde{J}(\sqrt{3}\omega_H) \quad (5)$$

In eq 5, the classical $[4\tilde{J}(2\omega_H)+\tilde{J}(\omega_H)]$ has been substituted by $5\tilde{J}(\sqrt{3}\omega_H)$, which appears to be an excellent approximation.[24] By use of this approximation, it turns out that this low-frequency part of the intramolecular dispersion curve can be decomposed into two Lorentzian curves. In this way, R_1 is fitted according to

$$R_1^{dip} = A_1^{dip}\left[\frac{5}{1+(\sqrt{3}\omega_H\tau_{c_1}^{dip})^2}\right] + A_2^{dip}\left[\frac{5}{1+(\sqrt{3}\omega_H\tau_{c_2}^{dip})^2}\right] \quad (6)$$

Again, A_i^{dip} involves the factor $2\tau_{c_i}^{dip}$. The A_i^{dip} and $\tau_{c_i}^{dip}$ values are gathered in Table 2.

As it is certain that one is dealing with intramolecular dipolar interactions, the correlation times are meaningful and reflect the reorientation of water molecules. Obviously, the largest

dx.doi.org/10.1021/jp205456g |J. Phys. Chem. A 2011, 115, 9941–9946

Table 3. Whole Set of Parameters Deduced from Analysis of Dispersion Curves[a]

	filling degree		
	80%	60%	40%
$\tau_{c_1}^{dip}$ (ns)	46 321	46 653	45 204
A_1^{dip} (s^{-1})	92.3	116.0	148.3
$\tau_{c_2}^{dip}$ (ns)	8514	8347	9127
A_2^{dip} (s^{-1})	19.4	23.8	32.3
τ_c^{inter} (ns)	832	857	764
A^{inter} (s^{-1})	1.0	1.1	2.1
$\tau_{c_1}^{para}$ (ns)	0.118	0.111	0.111
A_1^{para} (s^{-1})	0.122	0.186	0.286
$\tau_{c_2}^{para}$ (ns)	0.001	0.002	0.005
A_2^{para} (s^{-1})	0.058	0.045	0.056

[a] Pertaining to the three samples with the same notation as in Tables 1 and 2 and with two additional parameters, A^{inter} and τ_c^{inter}, for the low-frequency intermolecular contribution.

correlation time corresponds to water strongly interacting with the pore surface. The other correlation time, although smaller, is still very large and is therefore also associated with surface effects, corresponding probably to a second hydration layer. It can be mentioned that similar results were obtained without the data from $T_{1\rho}$ measurements. Therefore, although these latter data do not reveal an additional motion, they probably lead to more accurate parameters.

Whole Dispersion Curve. Now that the major features of the recovery curves have been understood, it is tempting to perform a global fit on the H_2O full dispersion curve, which will involve five Lorentzian functions: two for the intramolecular dipolar interactions (at low frequency), one for the intermolecular contribution (which is the sole contribution at low frequency in the HOD dispersion curve), and two for paramagnetic relaxation. The global fit of the 80% sample yields results very close to those of Tables 1 and 2 and also the two parameters (amplitude and correlation time) of a Lorentzian function that seems to accommodate the low-frequency intermolecular contribution. Owing to the quality of the global fit for the 80% sample, the same procedure could be applied with some confidence to the other two samples (let us recall that, in those cases, HOD dispersion curves are not available). The procedure was indeed successful in the sense that we obtained similar correlation times. Moreover, concerning the amplitudes, they vary as expected with the filling degree. All the parameters deduced from these fits are gathered in Table 3. The agreement between experimental data and the recalculated global dispersion curves is excellent, as shown in Figure 7.

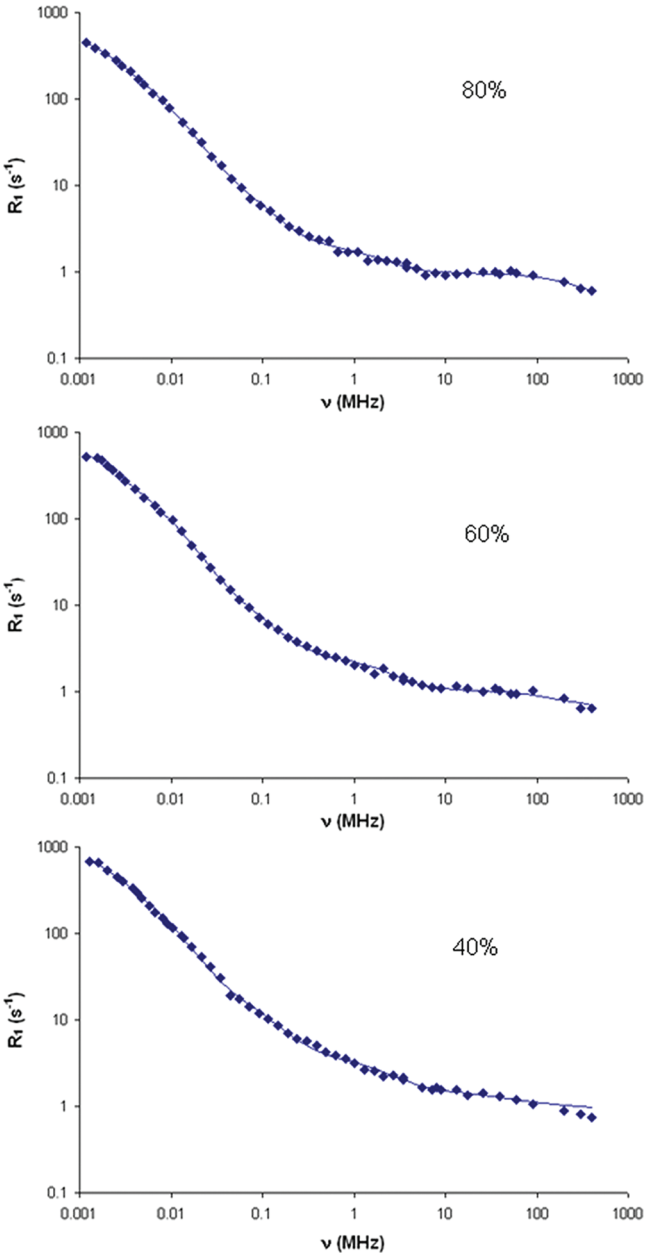

Figure 7. Experimental H_2O dispersion curves (◆) at the three filling degrees along with the continuous curves recalculated with the parameters of Table 3.

DISCUSSION AND CONCLUSION

In this work, we have been more interested in water behavior than in surface properties. Thanks to adequate instrumentation, we were able to obtain full recovery curves (i.e., covering the range 0−400 MHz). This has proven invaluable for deciphering the different types of water along with their properties. The correlation times have been discussed in the previous section and they should allow us first to separate intergranular water from water within the pores, with, however, one uncertainty about this separation for what we called (A_1^{para}, $\tau_{c_1}^{para}$). In order to lift this doubt and to derive further information, we can calculate, for each component i, the quantity $A_i/2\tau_{c_i}$, which is the amount of the i component multiplied by the factor characteristic of the relevant mechanism. In Table 4, these quantities are denoted by primes, and their ratio is evidently meaningful only if they arise from the same mechanism. The factor characteristic of the relaxation mechanism will therefore disappear and one is simply left with the relative proportion.

We notice that all A' values, except $A_2^{para\prime}$, increase when the filling degree decreases. This behavior is characteristic of water inside the pore for the following reasons. In Figure 7, we can observe that R_1 at zero frequency increases when the filling degree decreases. On the other hand, it is obvious that R_1 for water inside the pores is much larger than for intergranular water.

Table 4. Pertinent Parameters Extracted from Data of Table 3

	filling degree		
	80%	60%	40%
$A_1^{dip\prime} = A_1^{dip}/2\tau_{c_1}^{dip}$ (s^{-2})	1.0×10^6	1.2×10^6	1.6×10^6
$A_2^{dip\prime} = A_2^{dip}/2\tau_{c_2}^{dip}$ (s^{-2})	1.1×10^6	1.4×10^6	1.8×10^6
$A^{inter\prime} = A^{inter}/2\tau_c^{inter}$ (s^{-2})	6.0×10^5	6.4×10^5	14.0×10^5
$A_1^{para\prime} = A_1^{para}/2\tau_{c_1}^{para}$ (s^{-2})	5.2×10^8	8.4×10^8	12.9×10^8
$A_2^{para\prime} = A_2^{para}/2\tau_{c_2}^{para}$ (s^{-2})	2.9×10^{10}	1.1×10^{10}	0.6×10^{10}
$A_2^{dip\prime}/A_1^{dip\prime}$	1.1	1.2	1.1
$A_2^{para\prime}/A_1^{para\prime}$	56	13	5

This suggests that the absolute quantity of water within the pores is the same (at these three filling degrees), whereas it is the amount of intergranular water that diminishes when the filling degree decreases. Consequently, as observed in Table 4, the A' values follow the R_1 increase for water within the pores, whereas the opposite behavior prevails for intergranular water ($A_2^{para\prime}$). This definitely proves that what we have called (A_1^{para}, $\tau_{c_1}^{para}$) corresponds to water within the pores. Incidentally, we observe that the intermolecular contribution (A^{inter}, τ_c^{inter}) follows the same trend. Now the ratio $A_2^{dip\prime}/A_1^{dip\prime}$ is constant and should consistently correspond to the proportion of the assumed two hydration layers within a given pore. Conversely, the ratio $A_2^{para\prime}/A_1^{para\prime}$ strongly decreases with the filling degree. This is in perfect agreement with the above considerations, according to which the quantity of water within the pores is constant for these three filling degrees.

In summary, we have found that the high frequency part (beyond 1 MHz) of the dispersion curve is exclusively intermolecular in nature and is dominated by paramagnetic relaxation. Conversely, the low-frequency part is dominated by intramolecular dipolar relaxation. In that part, the intermolecular contribution could be left aside by means of HOD dispersion curve. This led us to define three types of water within the pores: one layer around the surface (characterized by the longest correlation time), a second layer roughly in the same proportion as the first layer (characterized by a correlation time 5 times smaller), and more mobile water (as indicated by its correlation time around 0.1 ns) essentially subjected to paramagnetic relaxation. Finally, there exists a decreasing amount of free water (when the filling degree decreases) as recognized by its correlation time (around 1 ps), which is again subjected to paramagnetic relaxation.

■ ASSOCIATED CONTENT

Supporting Information. Justification of complete surfactant removal in the mesoporous material. This material is available free of charge via the Internet at http://pubs.acs.org.

■ AUTHOR INFORMATION

Corresponding Author
*E-mail Daniel.Canet@crm2.uhp-nancy.fr.

■ REFERENCES

(1) Kowalewski, J.; Mäler, L. *Nuclear Spin Relaxation in Liquids: Theory, Experiments and Applications*; Taylor & Francis: London, 2006.
(2) Canet, D. *Nuclear Magnetic Resonance: Concepts and Methods*; Wiley: Chichester, U.K., 1996.
(3) Noack, F. *Prog. Nucl. Magn. Reson. Spectrosc.* **1986**, *18*, 171–276.
(4) Kimmich, R. *NMR - Tomography, Diffusometry, Relaxometry*; Springer-Verlag: Berlin, Heidelberg, and New York, 1997.
(5) Watson, A. T.; Chang, C. T. P. *Prog. Nucl. Magn. Reson. Spectrosc.* **1997**, *31*, 343–386.
(6) Kimmich, R. *Chem. Phys.* **2002**, *284*, 253–285.
(7) Kimmich, R.; Anoardo, E. *Prog. Nucl. Magn. Reson. Spectrosc.* **2004**, *44*, 257–320.
(8) Beck, J. S.; Vartuli, J. C.; Roth, W. J.; Leonowicz, M. E.; Kresge, C. T.; Schmitt, K. D.; Chu, C. T.-W.; Olson, D. H.; Sheppard, E. W.; McCullen, S. B.; Higgins, J. B.; Schlenker, J. L. *J. Am. Chem. Soc.* **1992**, *114*, 10834–10843.
(9) Blin, J. L.; Lesieur, P.; Stébé, M. J. *Langmuir* **2004**, *20*, 491–498.
(10) Stapf, S.; Kimmich, R.; Seitter, R.-O.; Maklakov, A. I.; Skirda, V. D. *Colloids Surf.* **1996**, *115*, 107–114.
(11) Korb, J.-P.; Malier, L.; Cros, F.; Xu, S.; Jonas, J. *Phys. Rev. Lett.* **1996**, *77*, 2312–2315.
(12) Zavada, T.; Kimmich, R. *J. Phys. Chem.* **1998**, *109*, 6929–6939.
(13) Perrin, J.-C.; Lyonnard, S.; Guillermo, A.; Levitz, P. *Magn. Reson. Imaging* **2007**, *25*, 501–504.
(14) Kiihne, S.; Bryant, R. G. *Biophys. J.* **2000**, *78*, 2163–2169.
(15) Yemloul, M.; Steiner, E.; Robert, A.; Bouguet-Bonnet, S.; Allix, F.; Jamart-Grégoire, B.; Canet, D. *J. Phys. Chem. B* **2011**, *115*, 2511–2517.
(16) Steiner, E.; Yemloul, M.; Guendouz, L.; Leclerc, S.; Robert, A.; Canet, D. *Chem. Phys. Lett.* **2010**, *495*, 287–291.
(17) Meiboom, S.; Gill, D. *Rev. Sci. Instrum.* **1958**, *29*, 688–691.
(18) Mitchell, J.; Chandrasekera, T. C.; Johns, M. L.; Gladden, L. F.; Fordham, E. J. *Phys. Rev.* **2010**, *81*, No. 026101.
(19) Hausser, R.; Noack, F. *Z. Naturforsch.* **1965**, *20a*, 1668.
(20) Teng, C.-L.; Hong, H.; Kiihne, S.; Bryant, R. G. *J. Magn. Reson.* **2001**, *148*, 31–34.
(21) Halle, B.; Jóhannesson, H.; Venu, K. *J. Magn. Reson.* **1998**, *135*, 1–13.
(22) Belorizky, E.; Fries, P.; Guillermo, A.; Poncelet, O. *Chem. Phys. Chem.* **2010**, *11*, 2021–2026.
(23) Nordstiema, L.; Yushmanov, P. V.; Furó, I. *J. Chem. Phys.* **2006**, *125*, No. 074704.
(24) Koenig, S. H.; Schillinger, W. E. *J. Biol. Chem.* **1969**, *244*, 3283.